Cellulose (2017) 24:4807–4819
DOI 10.1007/s10570-017-1469-5

ORIGINAL PAPER

# Fabrication of homogeneous and enhanced soybean protein isolate-based composite films via incorporating TEMPO oxidized nanofibrillated cellulose stablized nano-ZnO hybrid

**Yutao Yan · Kaili Wang · Zhong Wang · Wolfgang Gindl-Altmutter · Shifeng Zhang · Jianzhang Li**

Received: 28 May 2017 / Accepted: 17 August 2017 / Published online: 23 August 2017


**Abstract** Soybean protein isolate (SPI) is well-suited to the preparation of composite films due to its abundance, renewability, biodegradability, and favorable film-forming capacity. In this study, different SPI-based composite films were prepared by incorporating nano-ZnO and 2,2,6,6-Tetramethylpiperidine 1-oxyl (TEMPO) oxidized nanofibrillated cellulose (TNFC) separately or together. Nano-ZnO was introduced to endow the films with multi-function capability, while TNFC was introduced to stabilize the nanoparticles. Both the macro optical characterization and micro scanning electron microscope with energy dispersive X-ray (SEM–EDX) analysis indicated that TNFC could significantly decrease nano-ZnO aggregation and improve its dispersibility in the SPI matrix due to the mechanical restriction and physical adsorption effect of TNFC to the nano-ZnO. In addition to the improved dispersibility, incorporating nano-ZnO and TNFC benefitted the mechanical properties and thermo stability of the SPI-based composite films. The tensile strength and Young's modulus increased by 73 and 57%, respectively, and the maximum degradation temperature increased by 10 °C, compared to that of the unmodified SPI film. These results can be attributed to the hydrogen bonds formed among SPI components, TNFC, and nano-ZnO, which were further examined by attenuated total reflectance-fourier transform infrared spectroscopy and X-ray diffraction analysis. After the incorporation of nano-ZnO, the SPI-based composite films also possessed excellent UV-shielding capacity and superior antimicrobial ability. To this effect, this work provides a valuable reference for nanoparticles dispersion and application in regards to polymer enhancement and multi-functionalization.

**Keywords** Soy protein isolate · Films · TEMPO oxidized nanofibrillated cellulose · Nano-ZnO · Improved dispersibility · Multi-functionalization

Y. Yan · K. Wang · Z. Wang · S. Zhang (✉) · J. Li
Ministry of Education Key Laboratory of Wooden Material Science and Application, Beijing Key Laboratory of Wood Science and Engineering, MOE Engineering Research Centre of Forestry Biomass Materials and Bioenergy, Beijing Forestry University, Beijing 100083, China
e-mail: shifeng.zhang@bjfu.edu.cn

W. Gindl-Altmutter
Department of Materials Science and Process Engineering, BOKU-University of Natural Resources and Life Science Vienna, Vienna, Austria
e-mail: wolfgang.gindl@boku.ac.at

## Introduction

Soy protein isolate (SPI), as a biopolymer derived from soy oil industry byproduct, is a popular research object for non-formaldehyde wood adhesive, biodegradable film, and food packing material

applications due to its abundance, renewability, biodegradability, and favorable film-forming capacity (González and Alvarez Igarzabal 2015; González et al. 2011; Kang et al. 2016; Liu and Li 2007; Song et al. 2011; Xu et al. 2015). It is a promising substitute for petroleum-based adhesives and packaging plastics. Its main drawbacks include its sensitivity to moisture and susceptibility to bacterial attack (Krochta and Mulder-Johnston 1997; Rhim et al. 2000) due to the numerous hydrophilic groups from the protein itself and the necessary incorporation of a hygroscopic plasticizer (Glycerin). Moreover, the relatively poor mechanical properties of SPI film severely restrict its wider application.

Numerous researchers have attempted to improve the properties of SPI-based composite films. Chemical cross-linking and physical blending with organic or inorganic fillers are the most common approaches. The aldehydic compounds formaldehyde (Chen et al. 2008), glyoxal (Vaz et al. 2005) and glutaraldehyde (Park et al. 2000) are typically applied to facilitate chemical cross-linking. Aldehyde-free agents such as sodium dodecyl sulfate (Rhim et al. 2002), stearic acid (Lodha and Netravali 2005), and ferulic acid can also be used. Nearly all these cross-linking methods endow SPI-based films with improved mechanical properties, and some result in enhanced water resistance (Chen et al. 2008; Rhim et al. 2002). The chemicals involved necessitate special reaction conditions, however, come at a high cost, and with environmental concerns. Physical incorporation of nanoparticles as reinforcements is an alternative, efficient way to improve the properties of different polymers without incorporating extra chemicals. Even better, the incorporation of nanoparticles may endow the polymers with special functions (Corbierre et al. 2001; Jiang et al. 2006; Johnsen et al. 2007; Odegard et al. 2005; Ramanathan et al. 2008). Different nanoparticles such as nano montmorillonite (Kumar et al. 2010), nano-$SiO_2$ (Ai et al. 2007), nano-clusters (Li et al. 2015), carbon nanoparticles (Li et al. 2016), carbon nanotubes (Zheng et al. 2007), and cellulose nanocrystals (Zhang et al. 2016) have been successfully incorporated to form SPI-based composite films. All of these nanoparticles improve the mechanical properties, water resistance, or thermal stability of the prepared SPI-based composite films to some extent. The incorporation of nano-$TiO_2$ into the SPI film also endows the film with better antibacterial capability (Wang et al. 2012). Unfortunately, most of the nanoparticles are prone to aggregation in the matrix (Chung et al. 2009), thus decreasing the reinforcement effect and weakening their special functions (Althues et al. 2007).

Making full use of nanoparticles without aggregation or precipitation during their introduction into polymers is highly challenging. Mechanical stirring and ultrasonic treatment are commonly used to improve the dispersion of nanoparticles in polymers (Chung et al. 2009), however these method are rendered impractical when the nanoparticle content is high, as the particles precipitate during the casting film-forming process. Other much more efficient methods have also been reported, such as surface modification by surfactants or coupling agents (Samaele et al. 2010; Zhang et al. 2006), coating the inorganic nanoparticles with organic polymers (Laurent et al. 2008; Yang et al. 2011), or in situ nanoparticle synthesis during composite processing (Grüneberger et al. 2015). Though these methods do improve the dispersibility of nanoparticles, the processes are complex and time-consuming.

Recently, using biopolymers for inorganic nanoparticles stabilization and dispersion has attracted great attention. Among them, nanocellulose as stabilizers for inorganic nanoparticles, scaffolds, carriers or templates for nanoparticles synthesis were most widely investigated. Li et al. immobilized $Fe_3O_4$ nanoparticles with NFC network for preparing nanopaper, and a uniform, flexible, magnetic, transparent nanopaper with outstanding mechanical performance was prepared (Li et al. 2013). Xiong et al. used nanofibrillated cellulose as the support and reductant for synthesis of $Fe_3O_4$/Ag nanocomposites with catalytic and antibacterial activity (Xiong et al. 2013). Au–Ag alloy nanoparticles have been synthesized by the co-reduction method and uniformly dispersed on cellulose nanocrystal (Shin et al. 2008) (Garrido et al. 2013). All above mentioned researches proved the efficiency of nanocellulose with regard to nanoparticles immobilization and dispersion. Therefore, in this study, a special kind of nanocellulose, 2,2,6,6-Tetramethylpiperidine 1-oxyl (TEMPO) oxidized nanofabrillated cellulose (TNFC), was applied as a template to immobilize nano-ZnO, and then integrated into the SPI polymer to prepare SPI/nano-ZnO/TNFC biocomposite films. TNFC was chosen not only because of its unique web-like structure and numerous excellent properties (e.g., high strength and

stiffness at low weight, renewability, biocompatibility, and biodegradability), but also due to the presence of charged groups (–$COO^-$) on the fiber surface (Saito et al. 2007) which possess excellent adsorption capacity to metal cations, metallic nanoparticles, and metallic oxides (Cai et al. 2009; Ifuku et al. 2009). The introduced hydrophilic charged groups and multi-hydroxyls allow the TNFC to blend well with the water-based SPI matrix, which have been proved by similar researches (Sun et al. 2015). As for nano-ZnO, due to excellent UV absorption and antimicrobial properties (Bajpai et al. 2011; Fu et al. 2015; Martins et al. 2013), its incorporation could endow the resultant SPI-based composite films with UV shielding and antimicrobial properties. Thus the aim of the present research is to fabricate homogeneous and enhanced SPI-based composite films via incorporating TNFC stablized nano-ZnO hybrid, evaluating the potentially stabilizing effect of TNFC on the dispersion of nano-ZnO in the SPI matrix. Further, the effects of the TNFC-nano-ZnO hybrid system on properties of the resultant SPI-based composite films are also analyzed including mechanical properties, structural changes, transparency, anti-microbial and thermal stability.

## Materials and methods

### Materials

SPI (95% protein) was purchased from Yuwang Ecological Food Industry Co., Ltd. (Shandong Province, China). Nano-ZnO (99.9%, d = 30 ± 10 nm) was purchased from Maikun Chemical Co., Ltd. (Shanghai, China). Glycerol (99% purity) and Sodium hydroxide (analytical grade) were purchased from Beijing Chemical Reagents Co., Ltd. (China). TNFC solution (solid content, 1.34%; diameter, 12–20 nm; carboxyl group content, 0.972 mmol $g^{-1}$) was obtained from Tianjing Haoyu Technology Co., Ltd. (China). Deionized water was used for the preparation of all solutions.

### Preparation of SPI/TNFC/nano-ZnO films

SPI-based composite films were prepared through a two-step casting method (Xu et al. 2015). First, the SPI solution was prepared by adding 5.0 g of SPI, 2.5 g of glycerol (50 wt% of SPI), and 95 g distilled water into a 250 mL beaker and magnetically stirring for 30 min. The pH of the produced homogenous suspension was adjusted to 9.0–10.0 with NaOH solution (10%, w/w), then heated in a water bath at 85 °C for another 30 min to obtain a translucent flavescent solution (Fig. 1a). Varying amounts of nano-ZnO (1, 2, 4% based on SPI weight) and/or TNFC (2.5, 5, 10% based on SPI weight) were added to the SPI solution and homogenized in a Fluka microhomogenizer for 2 min, then subjected to ultrasonic treatment (power 40%) for 10 min to obtain uniform dispersions. Next, the SPI solution (60 g) was poured into polystyrene plates and dried in an oven at 45 °C for 24 h. After that the formed films (with a thickness about 0.2 mm) were preconditioned at 50 ± 2% relative humidity (RH) and 25 ± 2 °C for 48 h before testing. Detailed formulation are listed in Table 1.

### Mechanical testing

The mechanical properties of SPI-based composite films were determined on a tensile testing machine (DCP-KZ300) at a deformation of 50 mm $min^{-1}$ and an initial gauge length of 50 mm. Each sample was cut into strips measuring 10 × 80 $mm^2$ and stress–strain curves were recorded for five replicates each (Xu et al.

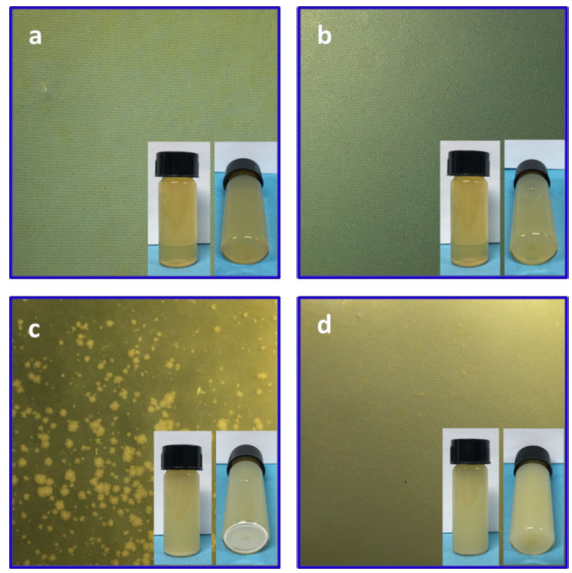


**Fig. 1** Optical characterization of different film-forming solution and SPI-based composite films, **a** SPI; **b** SPI + 5%TNFC; **c** SPI + 4%ZnO; **d** SPI + 5%TNFC + 4%ZnO

**Table 1** Formulation of different SPI/nano-ZnO/TNFC composite films

| Samples | SPI (g) | Glycerol (g) | Water (g) | TNFC (g) | Nano-ZnO (g) |
|---|---|---|---|---|---|
| SPI | 5 | 2.5 | 95 | 0 | 0 |
| SPI + 1%ZnO | 5 | 2.5 | 95 | 0 | 0.05 |
| SPI + 2%ZnO | 5 | 2.5 | 95 | 0 | 0.10 |
| SPI + 4%ZnO | 5 | 2.5 | 95 | 0 | 0.20 |
| SPI + 4%ZnO + 2.5%TNFC | 5 | 2.5 | 95 | 0.125 | 0.2 |
| SPI + 4%ZnO + 5%TNFC | 5 | 2.5 | 95 | 0.25 | 0.2 |
| SPI + 4%ZnO + 10%TNFC | 5 | 2.5 | 95 | 0.5 | 0.2 |
| SPI + 5%TNFC | 5 | 2.5 | 95 | 0.25 | 0 |

2015). The thickness and width were measured in three replicates with a digimatic micrometer and vernier caliper, respectively. The average values of tensile strength, elongation at break, and Young's modulus were calculated from the stress–strain curves.

### Scanning electron microscope with energy dispersive X-ray (SEM–EDX) analysis

The morphology of the surface and cross sections of films was observed using a SU8010 field emission scanning electron microscope (Hitachi Ltd., Japan) operating at an acceleration voltage of 5 kV. The films were frozen in liquid nitrogen and snapped immediately. In addition, the Zn element distributions on the cross section of different films were mapped by EDX spectra. The mapping thickness on the cross section was the entire film thickness 0.2 mm.

### Attenuated total reflectance-Fourier transform infrared (ATR-FTIR) spectroscopy

The film samples were directly examined by ATR-FTIR (Nicolet 6700 spectrometer, Thermo Scientific, USA) in the range of 4000–650 $cm^{-1}$ at 4 $cm^{-1}$ resolution for 32 scans with an ATR accessory equipped with a diamond crystal.

### UV–vis spectra

The transmittance of different films within the range of 200–700 nm was recorded on a TU-1901 UV–vis spectrophotometer (Beijing Purkinje General, Beijing, China) with a resolution of 2 nm.

### Thermo-gravimetric analysis (TGA)

The thermal stability of each film was assessed by TGA. Non-isothermal degradation measurements were gathered on a Q50 TGA device (TA Instruments, USA). Tests were run from room temperature to 700 °C at a heating rate of 10°C $min^{-1}$ under nitrogen atmosphere protection.

### Antibacterial and Antimold test

*S. aureus* (ATCC 6538) and *E. coli* (ATCC 25922) were used to examine the antibacterial activity of SPI films via disc diffusion method (Fu et al. 2015) with Luria–Bertani (LB) medium solid agar in Petri dishes. All the films were cut into pieces 6 mm in diameter, sterilized with UV light and placed on *S. aureus*-cultured agar and *E. coli*-cultured agar plates, then incubated at 37 °C for 24 h. A bacterial inhibition zone formed around the film after incubation.

To test the mold resistance of the SPI-based composite film, a easy method by placing the films in a desiccators at 92% relative humidity for 7 days after achieving balance.

### X-ray diffraction analysis (XRD)

The crystalline structures of different SPI-based composite films were investigated by XRD characterization with an XRD-6000 m (Shimadzu, Kyoto, Japan) in continuous scanning mode, operating at 40 kV and 40 mA. The samples were scanned from 5° to 55°(2θ) at 2°/min under CuKα radiation with a step interval of 0.02°.

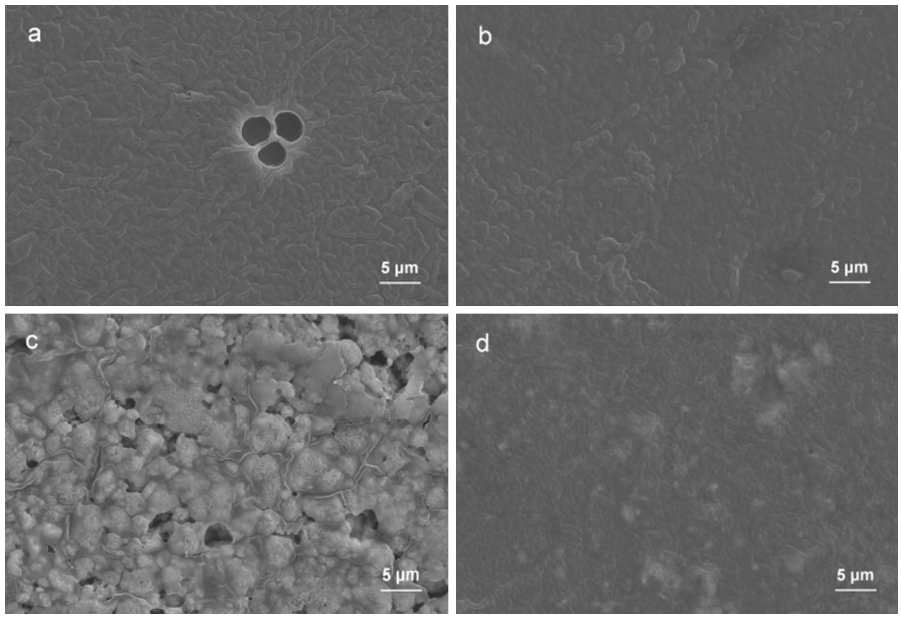


**Fig. 2** Surface SEM graphs of different SPI-based composite films, **a** SPI; **b** SPI + 5%TNFC; **c** SPI + 4%ZnO; **d** SPI + 5%TNFC + 4%ZnO

## Results and discussion

### Morphology characterization

#### *Optical characterization of SPI-based composite films*

Figure 1 shows the surface morphology of different SPI-based films and the film-forming solution under the optical camera. Clearly, the surface morphology varied considerably with different additives. When only TNFC was introduced, no obvious differences were found both regarding the films surface morphology and the solution state, which were smooth and homogenous (Fig. 1a, b). When nano-ZnO alone was incorporated, several white spots appeared on the film surface as a result of nano-ZnO aggregation. Aggregation also occurred in the film forming solution, as shown in Fig. 1c, where the solution turned from translucent to opaque and a layer of white nano-ZnO sedimentated on the bottom of the small bottle after standing for 8 h. However, when additionally TNFC was incorporated, a homogeneous film was obtained and no precipitates was found on the bottom of the bottle (Fig. 1d). These results indicated that TNFC helps disperse and stabilize the nano-ZnO in the SPI matrix, thus forming a uniform composite film.

#### *SEM–EDX analysis*

Micro analysis was performed by SEM–EDX to confirm the immobilization and stabilization effect of TNFC to nanoparticles. Figure 2 shows SEM images of the different SPI-based films. The surface of the pure film was smooth, but some small holes appeared at the magnification of 2000, which may result from gas bubbles occurring during the film formation. The smooth surface was still kept after the incorporation of TNFC, indicating the excellent dispersibility of TNFC in the SPI matrix, which was due to multi-hydroxyl groups and hydrophilic carboxyl on the TNFC surface, enhancing the interfacial compatibility between SPI matrix and TNFC. The surface of the only nano-ZnO-modified film was rather rough and numerous large, granular spots were observed (Fig. 2c), which could be attributed to the aggregation of nano-ZnO in the film. The surface became smooth again when TNFC was reintroduced (Fig. 2d), indicating an improved dispersion of nano-ZnO on the SPI-based composite film surface.

Figure 3 shows the cross section SEM graphs of SPI-ZnO composite films with and without TNFC. When only nano-ZnO was introduced (Figs. 3a), the

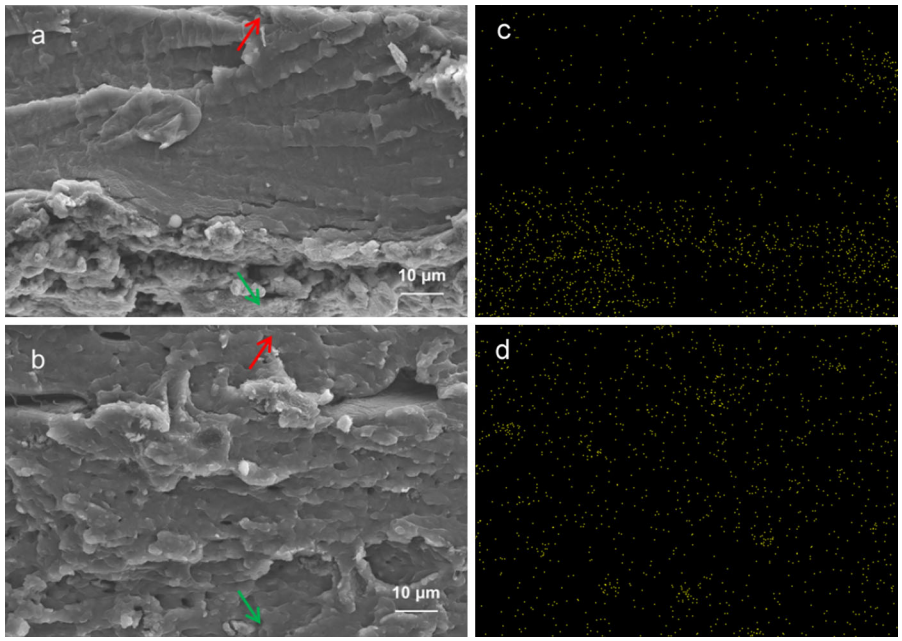


**Fig. 3** Cross section SEM graphs and EDX distributions of Zn element in different SPI-based composite films, **a** SPI + 4% ZnO; **b** SPI + 5%TNFC + 4% ZnO. *Note* the *red arrows* designate the upper surface of the films, whereas, the *green arrows* point to the bottom surface of the films. (Color figure online)

upper part of the film in thickness direction was smooth while the bottom part was rough and dense which may be due to nano-ZnO precipitation. Zn element distribution by EDX mapping proved this, where Zn mainly appeared on the bottom portion of the film's cross section in thickness direction (Fig. 3c). When TNFC was incorporated, the cross section morphology and Zn element distribution completely changed. As shown in the corresponding EDX mapping graph (Fig. 3d), the nano-ZnO was homogenously dispersed throughout the entire film cross section. These results indicate that TNFC exerts an excellent immobilization effect on nano-ZnO both on the surface and interior of SPI-based composite films. The improved dispersibility of nano-ZnO in the SPI matrix could be attribute to the following two reasons: first, the physical adsorption and support effect of TNFC to nano-ZnO derived from its active surface carboxyl groups and special web-like structure, which could prevent the nano-ZnO from aggregation and sedimentation; second, the excellent interfacial compatibility between TNFC and SPI enable well dispersion of the TNFC-nano-ZnO hybrid in the SPI matrix.

## Mechanical properties

Table 2 shows the mechanical properties of different SPI-based composite films. The tensile strength and Young's modulus of the film was increased as the increase of nano-ZnO addition, whereas the elongation at break was decreased, which are similar to recent reports on nanoparticle reinforced SPI films (Li et al. 2015; Li et al. 2016). When 2% nano-ZnO was incorporated, both the tensile strength and Young's modulus of the film increased especially the Young's modulus, from 173.58 MPa to 248.60 MPa, while the elongation at break decreased from 137.07% to 121.06% (Table 2). The variations of the mechanical properties was likely due to the strong interaction between nano-ZnO and the SPI molecules in the SPI matrix arising from hydrogen bonding effect formed between the surface multi-hydroxyl (-OH) from nano-ZnO and amino ($-NH_2$) from the SPI (Ai et al. 2007; Echeverría et al. 2014; Lu et al. 2004). The strong interaction endowed the film with improved strength while its restriction to the movement of SPI molecular decreased the elongation at break. When the nano-ZnO addition was further increased to 4%, however,

**Table 2** Tensile strength, Young's modulus and elongation at break of different SPI-based composite films with TNFC and nano-ZnO

| Samples | Tensile strength (MPa) | Young's modulus (MPa) | Elongation at break (%) |
|---|---|---|---|
| SPI | 6.17 ± 0.14 | 173.58 ± 11.90 | 133.07 ± 15.13 |
| SPI + 1% ZnO | 7.43 ± 0.05 | 204.18 ± 9.66 | 131.35 ± 8.37 |
| SPI + 2% ZnO | 7.87 ± 0.81 | 248.60 ± 23.83 | 121.06 ± 9.70 |
| SPI + 4% ZnO | 7.18 ± 0.23 | 206.85 ± 8.97 | 98.94 ± 10.72 |
| SPI + 4%ZnO + 2.5% TNFC | 7.88 ± 0.36 | 218.67 ± 5.91 | 47.60 ± 4.40 |
| SPI + 4%ZnO + 5% TNFC | 10.66 ± 0.19 | 272.25 ± 9.73 | 45.41 ± 6.72 |
| SPI + 4%ZnO + 10% TNFC | 13.36 ± 0.26 | 418.88 ± 13.70 | 23.66 ± 1.43 |
| SPI + 5% TNFC | 10.70 ± 0.24 | 285.03 ± 12.03 | 60.48 ± 3.40 |

all of the mechanical properties were decreased, which could be ascribe to the aggregation of excessive nano-ZnO in the SPI matrix and forming a strain concentration.

When TNFC was introduced into the 4% nano-ZnO enhanced SPI-based film, the reduced strength was recovered and increased with the increase of TNFC addition. When the TNFC addition reached 5%, the tensile strength increased by 48% and Young's modulus by 32% compared to that of only 4% nano-ZnO enhanced SPI-based film while the elongation at break significantly decreased. The further increased mechanical properties maybe result from the physical restriction of web-like TNFC to SPI molecular and the hydrogen bonding formed between the TNFC and SPI matrix.

Interestingly, the films enhanced by 5% TNFC and 4% nano-ZnO combined had similar strength and modulus as that of only 5% TNFC-enhanced SPI films, suggesting the dominating enhancement effect of TNFC when nano-ZnO was incorporated. The introduction of nano-ZnO is yet significant, however, as the incorporation of nanoparticles endows the prepared materials with special functions such as UV shielding and antibacterial capability. An effective combination of nanoparticles and TNFC may facilitate the preparation of homogenous and high-strength composite materials with multiple functions.

## ATR FT-IR analysis

The typical ATR FT-IR spectra of SPI-based composite films are shown in Fig. 4. The characteristic

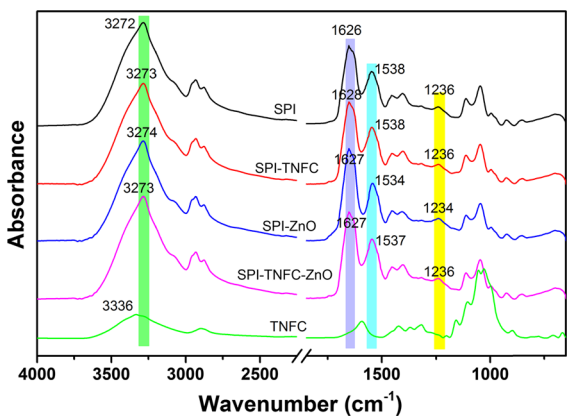


**Fig. 4** ATR FT-IR spectra of different SPI-based composite films

adsorption peaks at 3272 $cm^{-1}$ originate from O–H stretching and N–H bending, and the peaks at 2930 $cm^{-1}$ can be assigned to C–H stretching; 1038 $cm^{-1}$ for C–O stretching. The three characteristic peaks around 1626, 1538, and 1236 $cm^{-1}$ can be attributed to amide I (C=O stretching), amide II (N–H bending), and amide III (C–H and N–H stretching), respectively (Ciannamea et al. 2014; Tian et al. 2010). Compared with the unmodified SPI film, the absorption band intensity at 1626 $cm^{-1}$ increase slightly with the addition of the nano-ZnO or TNFC; this can be ascribed to the new hydrogen bonding formed between nano-ZnO and SPI matrix or TNFC and SPI (Ullah and Wu 2013). In addition, the amide II band related to N–H bending vibrations, which is sensitive to the environment of N–H group, could be used as a respond to the change of hydrogen bonding environment (Almutawah et al. 2007; Jung 2000). After the

incorporation of nano-ZnO and TNFC, the peak attributed to that amide II shifted to low wavenumber direction, indicating the interaction between the nano-ZnO and SPI matrix or TNFC and SPI matrix. Such interactions are very beneficial for the dispersion of nano-ZnO in the SPI solution, and for preventing nano-ZnO from aggregation during the film forming process.

According to the abovementioned SEM–EDX analysis and mechanical properties discussion we could deduce that the improved dispersibility of nano-ZnO in the SPI matrix and increased mechanical properties after incorporation of TNFC was not only due to the physical support and absorption effect, but also due to the hydrogen bonding among TNFC, nano-ZnO and SPI matrix. The possible interaction mechanism among TNFC, nano-ZnO and SPI are illustrated in Fig. 5.

## XRD analysis

The crystallinity structure properties of different SPI-based composite films were investigated by XRD as shown in Fig. 6. The unmodified SPI film showed distinct diffraction peaks at about 2θ ≈ 9.0° and 20° corresponding to the typical α-helix and β-sheet structures of the SPI secondary conformation, respectively (Chen et al. 2013; Li et al. 2016; Wang et al. 2012). The characteristic peaks of the cellulose at 2θ ≈ 16° and 22° (Aulin et al. 2012; Xiao et al. 2016) were overlapped with the SPI characteristic peaks when TNFC was introduced into the SPI matrix, but it is still visible due to a shoulder at 2θ ≈ 22° (Fig. 6, the green circles), implying good chemical compatibility and physical distribution of the TNFC in the composites (Salarbashi et al. 2016).

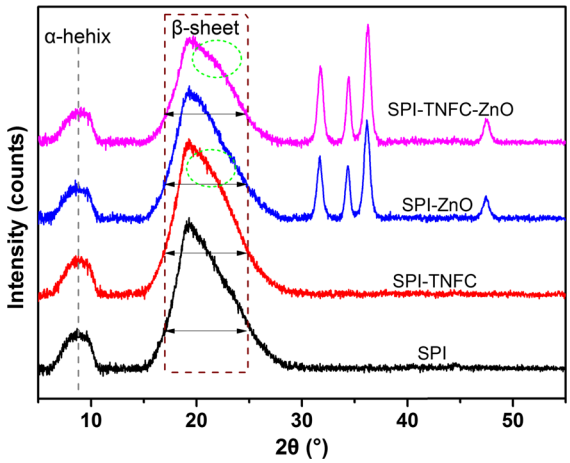


**Fig. 6** XRD patterns of different SPI-based composite films (*green dashed circles* indicate shoulder caused by the 200 reflection of cellulose I from TNFC)

When nano-ZnO was introduced into the SPI film, the typical ZnO crystallite peaks at 2θ ≈ 31.8°, 34.5°,

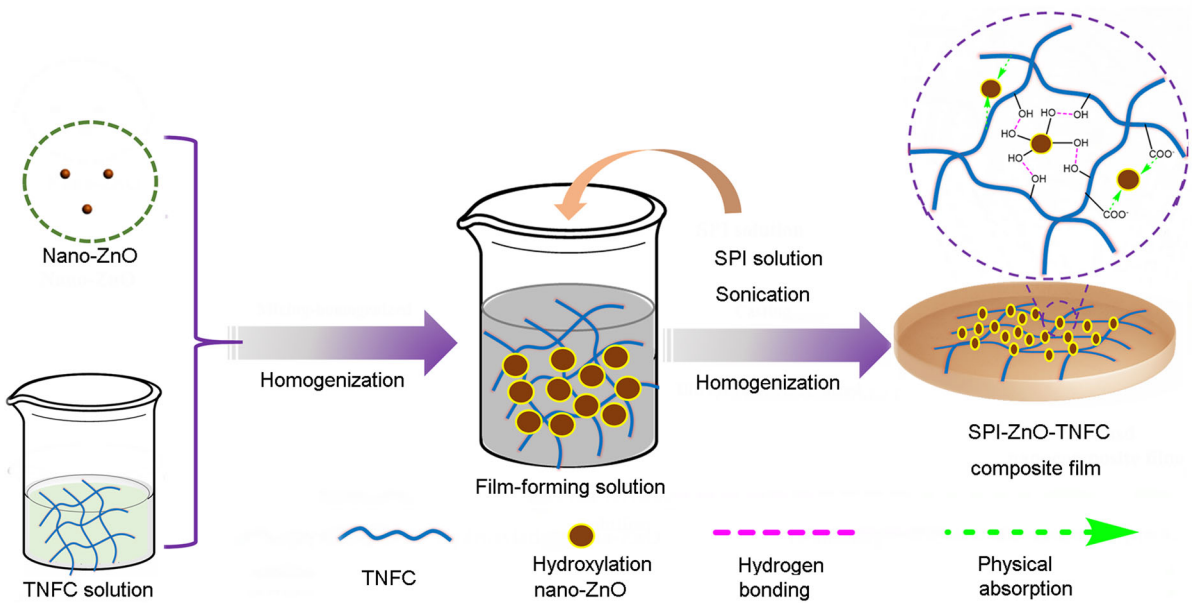


**Fig. 5** Mechanism of the improved dispersibility and mechanical properties

36.2°, and 47.8° (Bagheri and Rabieh 2013; Fu et al. 2015) were retained in the XRD pattern, indicating that the hexagonal structure of the nano-ZnO was not affected by ultrasonic-blending in the SPI hybrid matrix (Salarbashi et al. 2016). However, the intensity of the peak at $2\theta \approx 20°$ belonged to the crystalline domains (β-sheet) of SPI became weaker compared to the pure SPI film, indicating the change of SPI molecules conformation (Kang et al. 2016), which could be attributed to the hydrogen bonding interaction between nano-ZnO and SPI matrix. Similar behavior had also been reported by Wang et al. when they introduced titanium dioxide ($TiO_2$) into the SPI film (Wang et al. 2012). When TNFC was further incorporated, the intensity of the peak decreased much more obvious, indicating the interaction between TNFC and the nano-ZnO-SPI system. The interfacial interactions among nano-ZnO, TNFC and SPI matrix originated from hydrogen bonding under effective nano-ZnO dispersion is in accordance with the FT-IR analysis.

## UV–vis analysis

As shown in Fig. 7, the nano-ZnO ultraviolet shielding performance of the samples were favorable; when only 1% was added, UV below 340 nm could be fully blocked by the SPI-based film. Up to 2%, UV below 370 nm could be completely blocked. Upon 4% addition, all UV light was blocked. In other words, the composite SPI films possessed excellent UV shielding capacity, similar results have been also observed for CMC/ZnO nanocomposite film (Yu et al. 2009). When 5% TNFC was incorporated, however, the UV shielding ability of the film decreased compared to the film with only 4% nano-ZnO incorporated. This phenomenon indicates that the cause of UV shielding is two-fold: The UV absorption of nano-ZnO and the decreased blocking effect of the aggregated nano-ZnO particles due to the improvement in dispersibility.

In addition to the increased UV absorption, the incorporation of nano-ZnO also greatly affected visible light absorption. As shown in Fig. 7, the transmittance of films in the visible light region decreased with increase in nano-ZnO concentration. When the nano-ZnO addition reached 4%, the transmittance of the film was only 11% at wavelength of 700 nm; this is likely due to the yellowish but

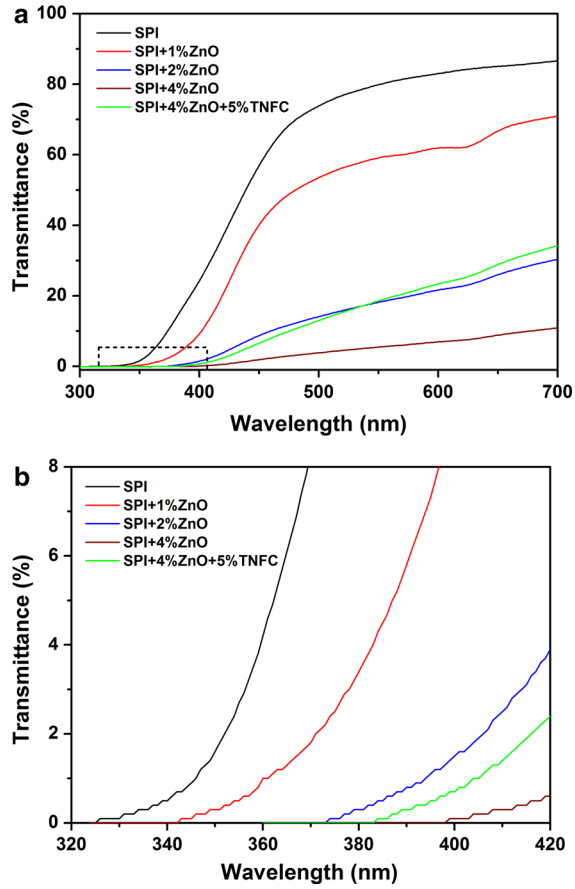


**Fig. 7** UV–vis absorption spectra of different SPI-based composite films. **a** original figure; **b** partial enlargement figure with the wavelength between 320 and 420 nm

translucent appearance of the film and the increased aggregation of nano-ZnO (Fig. 1c). However, when 5% TNFC was incorporated, the transmittance increased to 34% at wavelength of 700 nm attributable to the reduced scattering and improved dispersion of nano-ZnO in the film at the same concentration. These observations further verify the capacity of TNFC in improving the dispersion of nanoparticles.

## Antibacterial and Antimold analysis

The antibacterial activity of the pure SPI film and TNFC/nano-ZnO-incorporated SPI films against *E. coli* and *S. aureus* are shown in Fig. 8. As shown in Fig. 8a, no inhibition zones were detected against *E. coli* regardless of which SPI film was used, indicating the low antibacterial activity of SPI films

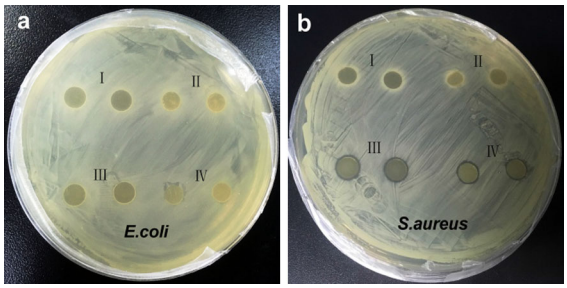


**Fig. 8** Inhibition zone test of the SPI-based composite films against. **a** E. coli and **b** *S. aureus*. *I* SPI; *II* SPI + 5%TNFC; *III* SPI + 4%ZnO; *IV* SPI + 5%TNFC + 4%ZnO

against *E. coli*. Some changes occurred in the round SPI pieces, however: Their shape became much smaller and the edges were integrated into the culture medium (Fig. 8a II and IV), which was especially obvious for the hydrophilic TNFC enhanced films. This may have occurred due to the dissolving of the SPI into the medium.

As for *S. aureus*-cultured agar, no inhibition zones were found around the unmodified SPI film or TNFC-SPI film similar to the *E. coli*-cultured agar. Conversely, obvious inhibition zones appeared when nano-ZnO was incorporated, indicating that nano-ZnO does have antibacterial activity towards *S. aureus*. Though the antibacterial mechanism of nano-ZnO is unknown, it is generally believed that the film can release ZnO or $Zn^{2+}$ into the medium that is further penetrated through the cell wall and reacts with the interior components of cells, thus inactivating them (Kanmani and Rhim 2014; Shankar et al. 2015). The better antibacterial activity of the films against *S. aureus* than against *E. coli* is in agreement with previous reports which suggest that variations in cell wall structures are responsible for the difference (Fu et al. 2015; Nafchi et al. 2012).

In a previous report, Xu et al. proved that modification can also endow these films with resistance to mold (Xu et al. 2015). In this study, all films (20 mm × 20 mm) were placed in desiccator at 92% RH for 1 week to determine their mold resistance (Fig. 9). The unmodified SPI film and TNFC (Fig. 9a, b) incorporated SPI film mildewed extensively while the nano-ZnO incorporated SPI films (Fig. 9c, d) had only small areas of mold, which indicated the superior antimold activity of nano-ZnO. The films also varied considerably in shape after 1 week. Films with TNFC

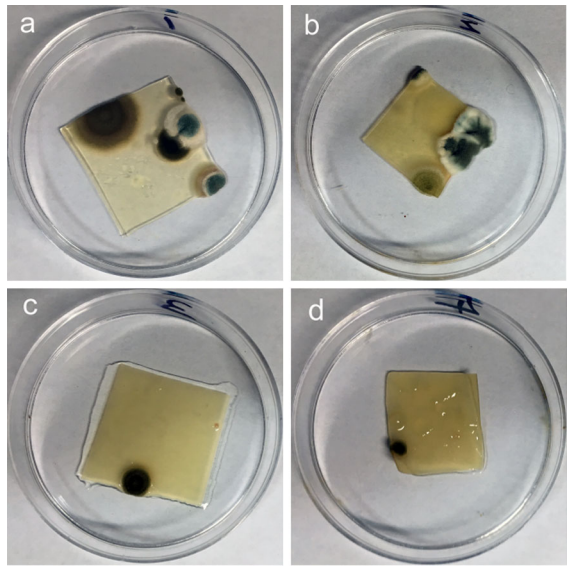


**Fig. 9** Morphology of different SPI-based composite films after 1 week in in desiccator at 92% relative humidity, **a** Unmodified SPI film; **b** SPI + 5%TNFC film; **c** SPI + 4%ZnO film; **d** SPI + 5%TNFC + 4%ZnO film

(Fig. 9b, d) maintained their original shapes fairly well while those without (Fig. 9a, c) swelled considerably. These changes may have been due to mold breaking the hydrogen bonds between the SPI film components (Xu et al. 2015). In addition to the hydrogen bonding effect, the web-like TNFC in the SPI matrix likely also mechanically constrained the movement of SPI molecules. These results altogether suggest that the incorporation of nano-ZnO endows SPI-based films with better antimold activity while TNFC improves their mechanical properties.

## TGA analysis

Figure 10 shows the TG and DTG curves of the SPI-based composite films. All films showed some amount of weight loss before 100 °C due to the evaporation of water. After that, there were two main weight loss stages as temperature increased: From 100 to 214 °C mainly due to the degradation of glycerol, and from 214 to 450 °C due to the backbone peptide degradation of SPI (Dash and Swain 2013; Xu et al. 2015). The different SPI films exhibited different maximum degradation temperatures and residues (Table 3), however. When 5% NFC was added, $T_{max2}$ was significantly increased from 288.68 to 298.68 °C,

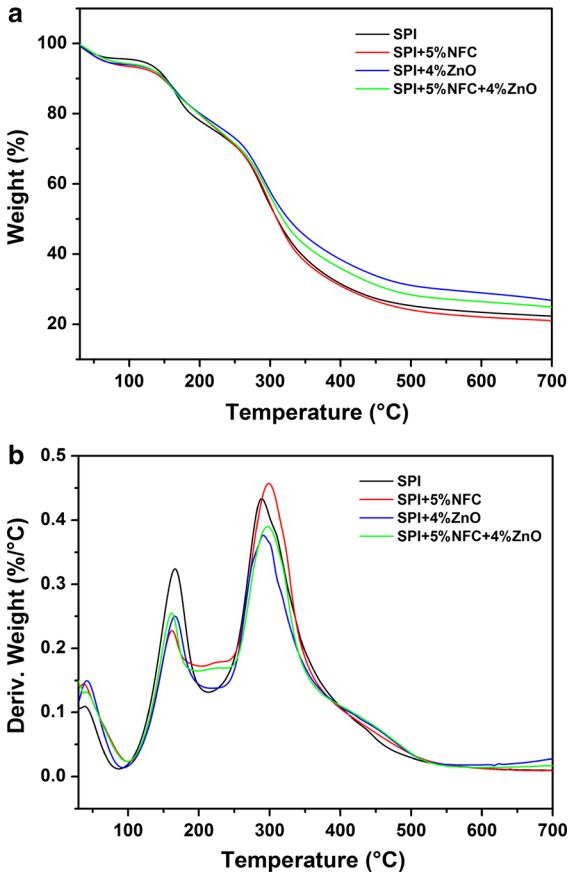


**Fig. 10** **a** TG and **b** DTG curves of the SPI-based composite films under nitrogen atmosphere

indicating that TNFC substantially improves the films thermal stability. This observation makes a difference from the results reported by Kang (2016) whose study showed that the introduction of microcrystalline cellulose had no influence on the thermal stability of the SPI-based film. The improved thermal stability may be attributable to the hydrogen bonds formed between TNFC and the SPI molecular chain due to the abundant hydrophilic groups (Wu and Zhang 2001). The incorporation of nano-ZnO also improved the films' thermal stability. When nano-ZnO was incorporated, the residues of the films were significantly increased(Table 3), which was due to the excellent thermal stability of nano-ZnO. However, when NFC was incorporated, the residues of the films were decreased which was mainly due to the full degradation of TNFC.

## Conclusions

In this study, homogenous and functional SPI-based composite films were prepared by incorporating nano-ZnO particles in combination with TNFC. Both marco optical characterization and micro SEM–EDX analysis indicated a favorable immobilization effect of TNFC to the nano-ZnO and a high degree of dispersibility in the resulting films. When 5% NFC and 4% nano-ZnO were introduced, the tensile strength of the film increased by 73% and the modulus by 57% compared to unmodified SPI film. Further, when the TNFC content reached 10%, the tensile strength was 13.36 MPa and modulus 418.88 MPa, more than twice those of pure SPI films. The films also showed improved thermo stability after modification.

These results may be attributed to the strong interactions between nano-ZnO particles, TNFC, and the SPI matrix more than simply the molecular restriction from the web-like structure of TNFC, as-indicated by ATR-IR, XRD characterization and TG analysis. The films also possess excellent UV shielding capacity and antimicrobial activities against the *S. aureus* and mold. To this effect, using TNFC as a template to immobilize and disperse various nanoparticles has significant potential in preparing multifunctional composite materials and coatings.

**Table 3** Thermal properties of different SPI-based composite films

| Samples | $T_i$ (°C) | $T_{max1}$ (°C) | $T_{max2}$ (°C) | Residue (%) |
|---|---|---|---|---|
| SPI | 137.84 | 165.49 | 288.68 | 22.33 |
| SPI + 5% TNFC | 137.09 | 160.74 | 298.97 | 21.07 |
| SPI + 4% ZnO | 138.18 | 164.77 | 291.02 | 26.82 |
| SPI + 4%ZnO + 5%TNFC | 137.20 | 160.67 | 298.23 | 24.94 |

**Acknowledgments** This research was supported by "The Fundamental Research Funds for the Central Universities" (No. 2016ZCQ01) and "the National Natural Science Foundation of China" (Project 51779005/E090301).

**Compliance with ethical standards**

**Conflicts of interest** The authors declare no conflict of interest.

## References

Ai F, Zheng H, Wei M, Huang J (2007) Soy protein plastics reinforced and toughened by SiO2 nanoparticles. J Appl Polym Sci 105:1597–1604

Almutawah A, Barker SA, Belton PS (2007) Hydration of gluten: a dielectric, calorimetric, and Fourier transform infrared study. Biomacromol 8:1601–1606

Althues H, Henle J, Kaskel S (2007) Functional inorganic nanofillers for transparent polymers. Chem Soc Rev 36:1454–1465

Aulin C, Salazar-Alvarez G, Lindström T (2012) High strength, flexible and transparent nanofibrillated cellulose–nanoclay biohybrid films with tunable oxygen and water vapor permeability. Nanoscale 4:6622

Bagheri M, Rabieh S (2013) Preparation and characterization of cellulose-ZnO nanocomposite based on ionic liquid ([C4mim]Cl). Cellulose 20:699–705

Bajpai SK, Chand N, Chaurasia V (2011) Nano zinc oxide-loaded calcium alginate films with potential antibacterial properties. Food Bioprocess Technol 5:1871–1881

Cai J, Kimura S, Wada M, Kuga S (2009) Nanoporous cellulose as metal nanoparticles support. Biomacromol 10:87–94

Chen L, Remondetto G, Rouabhia M, Subirade M (2008) Kinetics of the breakdown of cross-linked soy protein films for drug delivery. Biomaterials 29:3750–3756

Chen J, Chen X, Zhu Q, Chen F, Zhao X, Ao Q (2013) Determination of the domain structure of the 7S and 11S globulins from soy proteins by XRD and FTIR. J Sci Food Agric 93:1687–1691

Chung SJ, Leonard JP, Nettleship I, Lee J-K, Soong Y, Martello DV, Chyu MK (2009) Characterization of ZnO nanoparticle suspension in water: effectiveness of ultrasonic dispersion. Powder Technol 194:75–80

Ciannamea EM, Stefani PM, Ruseckaite RA (2014) Physical and mechanical properties of compression molded and solution casting soybean protein concentrate based films. Food Hydrocoll 38:193–204

Corbierre MK, Cameron NS, Sutton M, Mochrie SGJ, Lurio LB, Rühm A, Lennox RB (2001) Polymer-stabilized gold nanoparticles and their incorporation into polymer matrices. J Am Chem Soc 123:10411–10412

Dash S, Swain SK (2013) Effect of nanoboron nitride on the physical and chemical properties of soy protein. Compos Sci Technol 84:39–43

Echeverría I, Eisenberg P, Mauri AN (2014) Nanocomposites films based on soy proteins and montmorillonite processed by casting. J Membr Sci 449:15–26

Fu F, Li L, Liu L, Cai J, Zhang Y, Zhou J, Zhang L (2015) Construction of cellulose based ZnO nanocomposite films with antibacterial properties through one-step coagulation. ACS Appl Mater Interfaces 7:2597–2606

Garrido T, Etxabide A, Peñalba M, de la Caba K, Guerrero P (2013) Preparation and characterization of soy protein thin films: processing–properties correlation. Mater Lett 105:110–112

González A, Alvarez Igarzabal CI (2015) Nanocrystal-reinforced soy protein films and their application as active packaging. Food Hydrocoll 43:777–784

González A, Strumia MC, Alvarez Igarzabal CI (2011) Cross-linked soy protein as material for biodegradable films: synthesis, characterization and biodegradation. J Food Eng 106:331–338

Grüneberger F, Künniger T, Huch A, Zimmermann T, Arnold M (2015) Nanofibrillated cellulose in wood coatings: dispersion and stabilization of ZnO as UV absorber. Prog Org Coat 87:112–121

Ifuku S, Tsuji M, Morimoto M, Saimoto H, Yano H (2009) Synthesis of silver nanoparticles templated by TEMPO-mediated oxidized bacterial cellulose nanofibers. Biomacromol 10:2714–2717

Jiang H, K-s Moon, Li Y, Wong CP (2006) Surface functionalized silver nanoparticles for ultrahigh conductive polymer composites. Chem Mater 18:2969–2973

Johnsen BB, Kinloch AJ, Mohammed RD, Taylor AC, Sprenger S (2007) Toughening mechanisms of nanoparticle-modified epoxy polymers. Polymer 48:530–541

Jung C (2000) Insight into protein structure and protein–ligand recognition by Fourier transform infrared spectroscopy. J Mol Recognit 13:325–351

Kang HJ, Song XS, Wang Z, Zhang W, Zhang SF, Li JZ (2016) High-performance and fully renewable soy protein isolate-based film from microcrystalline cellulose via bio-inspired poly(dopamine) surface modification. ACS Sust Chem Eng 4:4354–4360

Kanmani P, Rhim JW (2014) Properties and characterization of bionanocomposite films prepared with various biopolymers and ZnO nanoparticles. Carbohydr Polym 106:190–199

Krochta JM, Mulder-Johnston D (1997) Edible and biodegradable polymer films: challenges and opportunities. Food technology (USA)

Kumar P, Sandeep KP, Alavi S, Truong VD, Gorga RE (2010) Preparation and characterization of bio-nanocomposite films based on soy protein isolate and montmorillonite using melt extrusion. J Food Eng 100:480–489

Laurent S, Forge D, Port M, Roch A, Robic C, Vander Elst L, Muller RN (2008) Magnetic iron oxide nanoparticles: synthesis, stabilization, vectorization, physicochemical characterizations, and biological applications. Chem Rev 108:2064–2110

Li Y et al (2013) Strong transparent magnetic nanopaper prepared by immobilization of Fe3O4 nanoparticles in a nanofibrillated cellulose network. J Mater Chem A 1:15278

Li K, Chen H, Li Y, Li J, He J (2015) Endogenous Cu and Zn nanocluster-regulated soy protein isolate films: excellent hydrophobicity and flexibility. RSC Adv 5:66543–66548

Li Y, Chen H, Dong Y, Li K, Li L, Li J (2016) Carbon nanoparticles/soy protein isolate bio-films with excellent

mechanical and water barrier properties. Ind Crops Prod 82:133–140
Liu Y, Li K (2007) Development and characterization of adhesives from soy protein for bonding wood. Int J Adhes Adhes 27:59–67
Lodha P, Netravali AN (2005) Thermal and mechanical properties of environment-friendly 'green' plastics from stearic acid modified-soy protein isolate. Ind Crops Prod 21:49–64
Lu Y, Weng L, Zhang L (2004) Morphology and properties of soy protein isolate thermoplastics reinforced with chitin whiskers. Biomacromol 5:1046–1051
Martins NCT et al (2013) Antibacterial paper based on composite coatings of nanofibrillated cellulose and ZnO. Colloids Surf Physicochem Eng Aspects 417:111–119
Nafchi AM, Alias AK, Mahmud S, Robal M (2012) Antimicrobial, rheological, and physicochemical properties of sago starch films filled with nanorod-rich zinc oxide. J Food Eng 113:511–519
Odegard GM, Clancy TC, Gates TS (2005) Modeling of the mechanical properties of nanoparticle/polymer composites. Polymer 46:553–562
Park S, Bae D, Rhee K (2000) Soy protein biopolymers cross-linked with glutaraldehyde. J Am Oil Chem Soc 77:879–884
Ramanathan T et al (2008) Functionalized graphene sheets for polymer nanocomposites. Nat Nanotechnol 3:327–331
Rhim JW, Gennadios A, Handa A, Weller CL, Hanna MA (2000) Solubility, tensile, and color properties of modified soy protein isolate films. J Agric Food Chem 48:4937–4941
Rhim JW, Gennadios A, Weller CL, Hanna MA (2002) Sodium dodecyl sulfate treatment improves properties of cast films from soy protein isolate. Ind Crops Prod 15:199–205
Saito T, Kimura S, Nishiyama Y, Isogai A (2007) Cellulose nanofibers prepared by TEMPO-mediated oxidation of native cellulose. Biomacromol 8:2485–2491
Salarbashi D, Mortazavi SA, Noghabi MS, Fazly Bazzaz BS, Sedaghat N, Ramezani M, Shahabi-Ghahfarrokhi I (2016) Development of new active packaging film made from a soluble soybean polysaccharide incorporating ZnO nanoparticles. Carbohydr Polym 140:220–227
Samaele N, Amornpitoksuk P, Suwanboon S (2010) Effect of pH on the morphology and optical properties of modified ZnO particles by SDS via a precipitation method. Powder Technol 203:243–247
Shankar S, Teng X, Li G, Rhim J-W (2015) Preparation, characterization, and antimicrobial activity of gelatin/ZnO nanocomposite films. Food Hydrocoll 45:264–271
Shin Y, Bae I-T, Arey BW, Exarhos GJ (2008) Facile stabilization of gold-silver alloy nanoparticles on cellulose nanocrystal. J Phys Chem C 112:4844–4848
Song F, Tang DL, Wang XL, Wang YZ (2011) Biodegradable soy protein isolate-based materials: a review. Biomacromol 12:3369–3380
Sun L, Chen W, Liu Y, Li J, Yu H (2015) Soy protein isolate/cellulose nanofiber complex gels as fat substitutes: rheological and textural properties and extent of cream imitation. Cellulose 22:2619–2627
Tian H, Wang Y, Zhang L, Quan C, Zhang X (2010) Improved flexibility and water resistance of soy protein thermoplastics containing waterborne polyurethane. Ind Crops Prod 32:13–20
Ullah A, Wu J (2013) Feather fiber-based thermoplastics: effects of different plasticizers on material properties. Macromol Mater Eng 298:153–162
Vaz CM, van Doeveren PFNM, Yilmaz G, de Graaf LA, Reis RL, Cunha AM (2005) Processing and characterization of biodegradable soy plastics: effects of crosslinking with glyoxal and thermal treatment. J Appl Polym Sci 97:604–610
Wang S-Y, Zhu B-B, Li D-Z, Fu X-Z, Shi L (2012) Preparation and characterization of TIO2/SPI composite film. Mater Lett 83:42–45
Wu Q, Zhang L (2001) Effects of the molecular weight on the properties of thermoplastics prepared from soy protein isolate. J Appl Polym Sci 82:3373–3380
Xiao S, Gao R, Gao L, Li J (2016) Poly(vinyl alcohol) films reinforced with nanofibrillated cellulose (NFC) isolated from corn husk by high intensity ultrasonication. Carbohydr Polym 136:1027–1034
Xiong R, Lu C, Wang Y, Zhou Z, Zhang X (2013) Nanofibrillated cellulose as the support and reductant for the facile synthesis of Fe3O4/Ag nanocomposites with catalytic and antibacterial activity. J Mater Chem A 1:14910
Xu F, Dong Y, Zhang W, Zhang S, Li L, Li J (2015) Preparation of cross-linked soy protein isolate-based environmentally-friendly films enhanced by PTGE and PAM. Ind Crops Prod 67:373–380
Yang C, Wu J, Hou Y (2011) Fe3O4 nanostructures: synthesis, growth mechanism, properties and applications. Chem Commun (Camb) 47:5130–5141
Yu J, Yang J, Liu B, Ma X (2009) Preparation and characterization of glycerol plasticized-pea starch/ZnO–carboxymethylcellulose sodium nanocomposites. Bioresour Technol 100:2832–2841
Zhang J, Gao G, Zhang M, Zhang D, Wang C, Zhao D, Liu F (2006) ZnO/PS core–shell hybrid microspheres prepared with miniemulsion polymerization. J Colloid Interface Sci 301:78–84
Zhang S, Xia C, Dong Y, Yan Y, Li J, Shi SQ, Cai L (2016) Soy protein isolate-based films reinforced by surface modified cellulose nanocrystal. Ind Crops Prod 80:207–213
Zheng H, Ai F, Wei M, Huang J, Chang PR (2007) Thermoplastic soy protein nanocomposites reinforced by carbon nanotubes. Macromol Mater Eng 292:780–788